VIP Gold Catalysis

DOI: 10.1002/anie.200801479

Trends in the Catalytic CO Oxidation Activity of Nanoparticles**

*Hanne Falsig, Britt Hvolbæk, Iben S. Kristensen, Tao Jiang, Thomas Bligaard, Claus H. Christensen, and Jens K. Nørskov**

Although extended gold surfaces are generally considered chemically inert[1,2] nanosized (< 5 nm) gold particles can be very effective catalysts for a number of oxidation reactions.[3–17] There are reports of similar size effects for silver catalysts.[18,19] The origin of the nanoeffects in the catalytic properties of these metals is widely debated,[15] and no consensus has been reached. Based on a set of density functional theory calculations of the full reaction pathway for CO oxidation over extended surfaces as well as over small nanoparticles of a number of metals, we show that although platinum and palladium are the most active catalysts for extended surfaces at high temperatures, gold is the most active for very small particles at low temperature. The calculations capture the special catalytic properties of nanosized particles observed experimentally, which allows the origin of the effect to be analyzed.

Herein, we focus on intrinsic metal effects; that is, we do not include additional possible effects that involve the support. It is not that such effects may not be important,[5,20,21] but it is useful to first establish the intrinsic metal effects,[15] in particular as it has been shown experimentally that nanostructured gold with no support is also catalytically active.[22,23] The key feature of our analysis is that we compare catalytic activities of different transition and noble metals for one specific reaction, the CO oxidation.

The CO oxidation reaction on close-packed fcc(111) surfaces was considered initially, which will give a dominant contribution to the total catalytic rate over large metal particles. We consider the following elementary reactions:

$$CO + * \rightleftharpoons CO* \quad \text{(R1)}$$

$$O_2 + * \rightleftharpoons O_2* \quad \text{(R2)}$$

$$O_2* + * \rightleftharpoons 2\,O* \quad \text{(R3)}$$

$$O* + CO* \rightleftharpoons CO_2 + 2* \quad \text{(R4)}$$

For the metals we consider herein, Reactions (R1) and (R2) are unactivated and fast, and we assume that these two reactions are in equilibrium. This means that we are limited to temperatures high enough that desorption is also fast. The possible formation of an oxide layer on the more reactive metals is neglected.

The forward and reverse rate constants of the Reactions (R3) and (R4) are given by $k_i = \nu_i \exp[-\Delta G_{ai}/kT] = \nu_i \exp[-(E_{ai} - T\Delta S_{ai})/kT]$, where ν_i is a prefactor, E_{ai} is the activation energy, k is the Boltzmann constant, and T is the absolute temperature. The activation energies are $E_a = \max(E_{TS} - E_{IS}, 0)$ where E_{IS} is the initial state energy and E_{TS} is the transition-state energy. ΔS_{ai} is the entropy difference between the transition state and the initial state. The entropy of adsorbed species are assumed to be zero, and the gas-phase entropies are taken from Ref. [24]. The adsorption energies of the different species E_{CO}, E_{O_2}, and E_O and the transition state energies are given with respect to the gas-phase molecules.

Assuming the prefactors and adsorption entropies are independent of the metal, there are five metal-dependent parameters determining the kinetics: E_{CO}, E_{O_2}, E_O, E_{TS3}, and E_{TS4}. The transition-state energies are, however, found to scale linearly with the adsorption energies, as shown for E_{TS3} and E_{TS4} in Figure 1 a and b. Such Brønsted–Evans–Polanyi (BEP) relations are found quite generally for surface reactions.[25] Furthermore, the O_2 adsorption energy scales with the O adsorption energy (Figure 1 c). This means that the adsorption energies E_{CO} and E_O can be viewed, to a first approximation, as the only independent variables characterizing the metal in the microkinetic model. Owing to the low number of elementary reactions, it is possible to find an analytical solution for this microkinetic model. Herein, we use instead the more general method of a so-called Sabatier analysis to find an upper bound to the overall reaction rate.[26]

The Sabatier rate[26] is the rate the reaction will have if all coverages are optimum for each elementary reaction step. Such conditions may not be obtainable in reality, but the Sabatier rate still provides an exact upper bound to the steady-state rate under any reaction conditions. The Sabatier rate is also an upper bound on the rate when islanding is included, as that will decrease the number of possible reaction centers to the length of the boundary between different phases.[27] The Sabatier rate thus forms a good measure of the intrinsic ability of a given metal surface to catalyze the reaction in question. The metal with the highest Sabatier rate is taken herein as being the best catalyst.

[*] Dr. B. Hvolbæk, I. S. Kristensen, T. Jiang, Dr. T. Bligaard, Prof. J. K. Nørskov
Center for Atomic-scale Materials Design, Department of Physics, Technical University of Denmark, DK-2800 Lyngby (Denmark)
Fax: (+45) 4593-2399
E-mail: norskov@fysik.dtu.dk
H. Falsig, Prof. C. H. Christensen
Center for Sustainable and Green Chemistry, Department of Chemistry, Technical University of Denmark
DK-2800 Lyngby (Denmark)

[**] The Center for Sustainable and Green Chemistry is supported by the Danish National Research Foundation, and the Center for Atomic-scale Materials Design is supported by the Lundbeck Foundation. In addition we thank the Danish Research Council for the Technical Sciences and the NABIIT program for financial support, and Danish Center for Scientific Computing for computer time.

Supporting information for this article is available on the WWW under http://dx.doi.org/10.1002/anie.200801479.

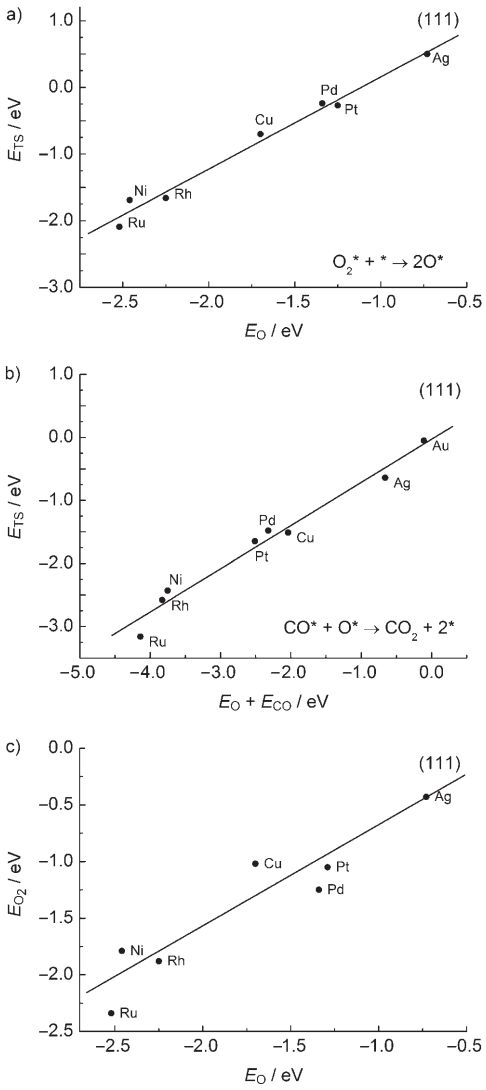

Figure 1. The BEP and scaling relations for different close-packed fcc(111)-surfaces. a) Calculated transition-state energies for O_2 dissociation (R3) as a function of oxygen adsorption energy. $E_{TS3} = 1.39\,E_O + 1.56$ eV. b) Calculated transition-state energies for adsorbed CO reacting with adsorbed O (R4) as a function of the sum of the O and CO adsorption energies. $E_{TS4} = 0.70(E_O + E_{CO}) + 0.02$ eV. c) The scaling of the O_2 adsorption energy with the oxygen adsorption energy $E_{O_2} = 0.89E_O + 0.17$ eV. For Pt(111,) the calculated reaction barrier $E_a = E_{TS} - (E_{CO} + E_O)$ for $CO^* + O^* \rightleftarrows CO_2 + 2^*$ is 0.85 eV, in good agreement with calculations.[28,29]

The rate of reaction for (R3) and (R4) are maximized if the reverse reactions are neglected. The Sabatier rate is therefore calculated from the forward rates:

$$r_3^+ = \theta_{O_2}\theta_* k_3^+ = \theta_{O_2}\theta_* \nu_3 \exp[-(E_{a3} - T\Delta S_{a3})/kT] \quad (1)$$

$$r_4^+ = \theta_O\theta_{CO} k_4^+ = \theta_O\theta_{CO} \nu_4 \exp[-(E_{a4} - T\Delta S_{a4})/kT] \quad (2)$$

where θ_{O_2} is the coverage of adsorbed oxygen molecules, θ_O is the coverage of adsorbed atomic oxygen, θ_{CO} is the coverage of adsorbed CO molecules, and θ_* is the coverage of free sites of the surface. The coverages will depend on the reaction conditions, temperature, reactant pressures, and conversion.

For the present case, the optimum coverages are found by first neglecting the coverage of atomic oxygen. Still assuming that (R1) and (R2) are in equilibrium, this gives:

$$\theta_*^{max} = \frac{1}{1 + K_1 p(CO) + K_2 p(O_2)} \quad (3)$$

where K_1 and K_2 are the equilibrium constants for (R1) and (R2), and $p(CO)$ and $p(O_2)$ are the partial pressures of CO and O_2. The optimum coverages of CO and O_2 have similar expressions, namely $\theta_{CO}^{max} = K_1 p(CO)\theta_*$ and $\theta_{O_2}^{max} = K_2 p(O_2)\theta_*$.

The Sabatier rates of each of the Reactions (R3) and (R4) are found by using the forward rates from (1) and (2) with the coverages of θ^{max}, θ_{CO}^{max} and $\theta_{O_2}^{max}$ from (3), and the coverage of θ_O^{max} set to one.

$$r_3^{S\,max} = k_3^+ \theta_{O_2}^{max} \theta_*^{max} \quad (4)$$

$$r_4^{S\,max} = k_4^+ \theta_{CO}^{max} \theta_O^{max} = k_4^+ \theta_{CO}^{max} \quad (5)$$

The Sabatier rate of forming CO_2 is determined by the lowest of the Sabatier rates of Reaction (R3) and (R4):

$$r_S = \min\{2r_3^{S\,max}, r_4^{S\,max}\} \quad (6)$$

where the factor of 2 stems from the stoichiometric number for (R3).

Figure 2 shows a contour plot of the Sabatier activity over close-packed surfaces. The Sabatier rate is calculated at $T = 600$ K, $P_{O_2} = 0.33$ bar and $P_{CO} = 0.67$ bar, corresponding to high-temperature CO oxidation conditions. The two-dimensional volcano plots show that, of the elemental metals, platinum and palladium are closest to the top. This agrees well with experimental evidence.[30] Platinum and palladium are

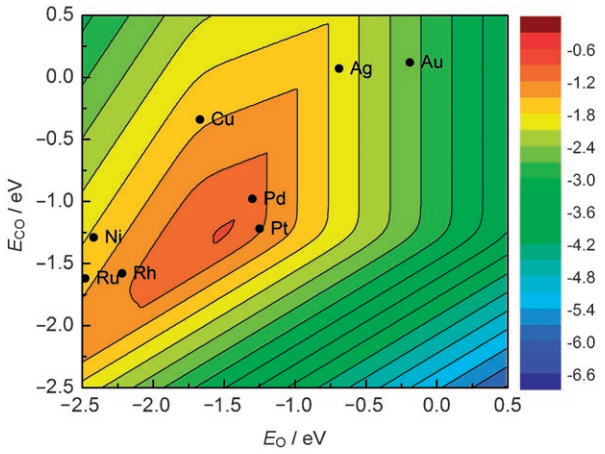

Figure 2. Contour plot of the Sabatier activity $A_S = kT\ln[r_S/\nu]$ over close-packed surfaces as a function of E_{CO} and E_O (ν is set to kT/h) under high-temperature conditions ($T = 600$ K, $P_{O_2} = 0.33$ bar, and $P_{CO} = 0.67$ bar). The values for different elemental metals can be taken from their indicated positions.

excellent CO oxidation catalysts, used for example in car exhaust after-treatment. This result is completely in line with DFT calculations and kinetic modeling by Grabow et al.[31] showing that at low temperatures, platinum without strain has a higher activity than either compressed (weaker bond energies) or expanded (stronger bond energies) platinum surfaces.

The reactivity of nanoparticles was then investigated. One important feature of nanoparticles is that the relative fraction of low-coordinate corner atoms to surface atoms is very large.[15,32] We concentrate herein on the reactivity of corner atoms, and model these by carrying out calculations for metal clusters containing twelve atoms, in the structure shown as inserts in Figure 3. All the twelve atoms in the cluster are held fixed with a lattice constant corresponding to the bulk value to mimic a geometrically constrained corner of a larger cluster, such as those in the range 2–5 nm studied experimentally. The calculations are thus more intended to model a general corner site on nanoparticles than specifically a twelve-atom cluster, as such small clusters will have much larger structural flexibility.[33]

It turns out that adsorption is considerably more exothermic on the twelve-atom clusters than on the close-packed surfaces. This makes it important to include another elementary reaction, as the coverage of molecular O_2 may be large enough such that an associative mechanism[34] may be important:

$$O_2{}^* + CO^* \rightleftharpoons CO_2 + O^* + {}^* \qquad \text{(R5)}$$

For the (111) surfaces, the weak bonding of O_2 combined with the reaction barrier for the process makes it unimportant for platinum[27] and less reactive metals.[35]

As for the fcc(111) surface, correlations between the transition state energies, E_{TS3}, E_{TS4}, and E_{TS5}, and the binding energies, E_O and E_{CO}, are found for the twelve-atom cluster. A scaling between E_{O_2} and E_O is also found. These relations are shown in Figure 3. The linear relations are similar to those of the close-packed surfaces (Figure 1), except that the adsorption energy axis has shifted. The adsorption energy of both CO and O are substantially more negative (exothermic adsorption) on the corner sites than on the close packed surfaces; compare for example, the adsorption energy of O on the (111) surfaces to those on the twelve-atom cluster: on the latter the bond is stronger by of the order 0.5 eV. The same trend is seen for molecular CO adsorption.

The expressions for the optimum coverages and the Sabatier rate for (R3) and (R4) are the same as for the fcc(111) surface. For (R5), the Sabatier rate is:

$$r_5^{S\max} = k_5^+ \theta_{CO}^{\max} \theta_{O_2}^{\max} \qquad (7)$$

Both Reaction (R3) and (R5) dissociate O_2, and can be followed by Reaction (R4) creating CO_2. The Sabatier activity is therefore given by:

$$r_S = \max\{2\min\{r_5^{S\max}, r_4^{S\max}\}, \min\{2r_3^{S\max}, r_4^{S\max}\}\} \qquad (8)$$

Figure 4 shows the contour plot of the Sabatier activity,

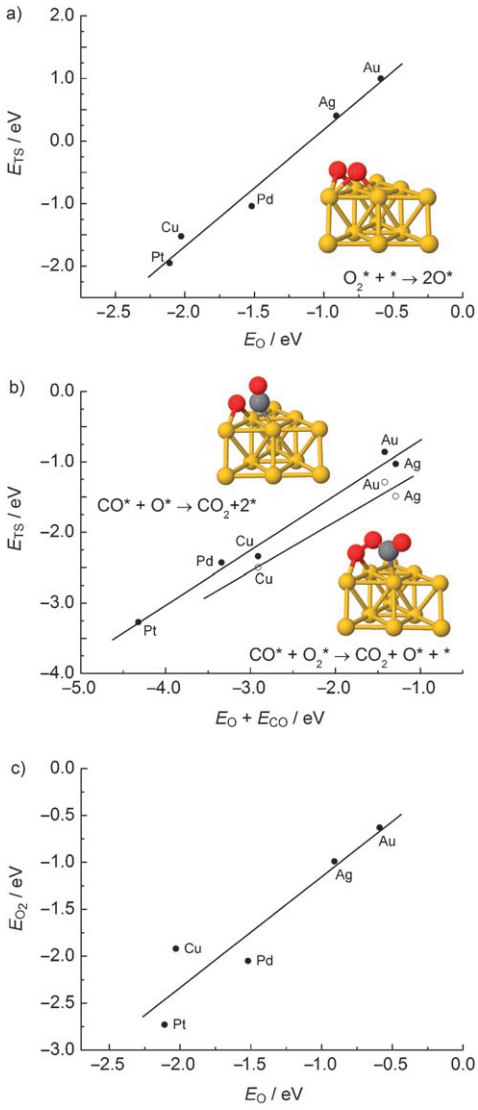

Figure 3. The BEP relations and scaling relation for different twelve-atom clusters. a) Calculated transition-state energies for O_2 dissociation (R3) as a function of oxygen adsorption energy. $E_{TS3} = 1.87\,E_O + 2.04$ eV. b) Calculated transition-state energies for adsorbed CO reacting with adsorbed O (R4) and O_2 (R5) as a function of the sum of the O and CO adsorption energies. $E_{TS4} = 0.78\text{-}(E_O + E_{CO}) + 0.09$ eV and $E_{T3S5} = 0.70(E_O + E_{CO}) - 0.44$ eV. c) The scaling of the O_2 adsorption energy with the O adsorption energy $E_{O_2} = 1.18\,E_O + 0.03$ eV. Transition states for the reactions on the Au_{12} cluster are shown as inserts.

$A_S = kT\ln[r_S/\nu]$. In this case, gold is closest to the top, followed by palladium and silver.

The results in Figure 2 and Figure 4 are in good agreement with available experimental observations.[3,32] It shows that the relative activities of different metals can be theoretically estimated, and it provides a clear picture of the catalyst properties determining the best catalysts in terms of the adsorption energies of the intermediates. The volcano plots of Figure 2 and Figure 4 can be viewed as an illustration of the Sabatier principle, with the important new feature that we know which adsorption energy that provides the optimum

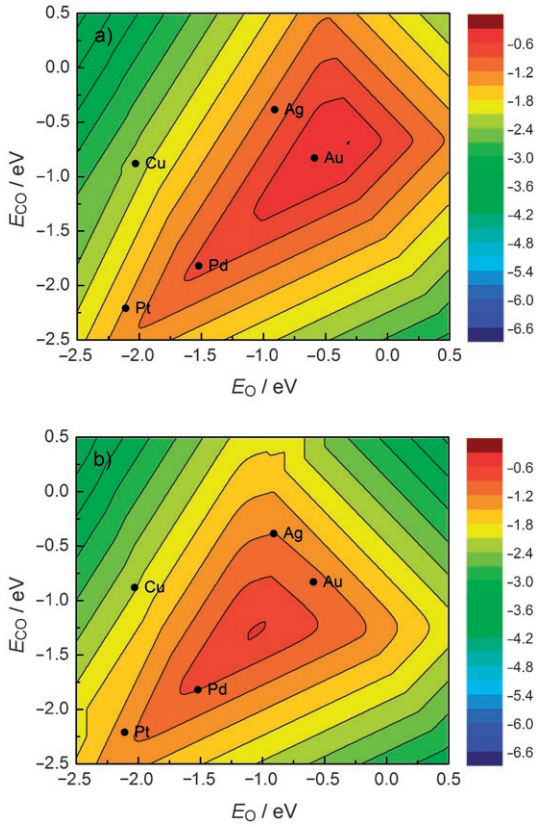

Figure 4. Contour plot of the Sabatier rate as a function of the CO and O adsorption energies on the twelve-atom clusters. The values for some elemental metals are shown. a) The activity under typical experimental conditions for CO oxidation by gold nanoparticles (T=273 K, P_{O_2}=0.21 bar, and P_{CO}=0.01) and b) the activity under high-temperature conditions (T=600 K, P_{O_2}=0.33 bar, and P_{CO}=0.67 bar).

catalyst. The position of the maximum in terms of adsorption energies depends slightly on the structure, which is related to the fact that the relationship between adsorption energy and activation energy is somewhat structure dependent. More importantly, it can be seen that the metals corresponding to a particular adsorption energy shift substantially depending on the coordination number of the metal atom. This is true for all the metals considered, and it is the dominant reason for gold becoming the best elemental catalyst for the low-coordinate sites. The shift is of the same order of magnitude as the difference between neighboring metals in the periodic table, explaining why it appears as if the top of the volcano has shifted by a little less than one place to the right in the periodic table from Figure 2 to Figure 4.

Comparing the volcanoes in Figure 2 and Figure 4, it is clear that for gold, the corner atoms will dominate over the close-packed surfaces for even quite large particles, as the value of r_S is many orders of magnitude larger in this case. For platinum, on the other hand, the difference is only about an order of magnitude. It should be noted that even for platinum, small particles could still be more active than larger ones, but only because the surface area per mass of catalyst is larger (scaling as d^{-1}).

The present analysis suggests that the more noble metals move to the maximum in the reactivity volcano when lower-coordinated metal atoms serve as active sites for the reaction. It suggests that similar results could be found for other reactions. For oxidation reactions, the best extended surface catalysts are already quite noble: platinum and palladium, and gold is the next, less reactive metal. For reactions involving less reactive molecules, such as N_2, we would expect that the best nanoparticle catalysts would not be gold but metals just to the right in the periodic table of the most active metals (ruthenium, iron) for this reaction, for example, cobalt or nickel. It is therefore possible that pronounced nanoeffects in catalysis is not restricted to gold.

In summary, we have modeled the special catalytic properties of nanosized particles observed experimentally, and analyzed the origin of the effect. The ability of the metal atoms to activate reactants change substantially as the coordination number of the active metal site is reduced at corners of metal particles. This model supports the hypothesis that part of the observed reactivity of gold nanoparticles is independent of the substrate.

Received: March 23, 2008
Published online: May 21, 2008

Keywords: carbon monoxide · density functional calculations · gold · heterogeneous catalysis · nanostructures

[1] D. T. Wickham, D. H. Parker, G. N. Kastanas, M. A. Lazaga, B. E. Koel, *Prepr. Am. Chem. Soc. Div. Pet. Chem.* **1992**, *37*, 1034.
[2] B. Hammer, J. K. Nørskov, *Nature* **1995**, *376*, 238–240.
[3] M. Haruta, T. Kobayashi, H. Sano, N. Yamada, *Chem. Lett.* **1987**, 405–408.
[4] M. Valden, X. Lai, D. W. Goodman, *Science* **1998**, *281*, 1647–1650.
[5] G. C. Bond, D. T. Thomson, *Catal. Rev. Sci. Eng.* **1999**, *41*, 319–388.
[6] M. A. P. Dekkers, M. J. Lippits, B. E. Nieuwenhuys, *Catal. Today* **1999**, *54*, 381.
[7] S. Carrettin, P. McMorn, P. Johnston, K. Griffin, G. J. Hutchings, *Chem. Commun.* **2002**, 696–697.
[8] S. Schimpf, M. Lucas, C. Mohr, U. Rodemerck, A. Brückner, J. Radnik, H. Hofmeister, P. Claus, *Catal. Today* **2002**, *72*, 63–78.
[9] S. Carrettin, P. McMorn, P. Johnston, K. Griffin, C. J. Kiely, G. A. Attard, G. J. Hutchings, *Top. Catal.* **2004**, *27*, 131–136.
[10] R. Meyer, C. Lemire, S. Shaikhutdinov, H. J. Freund, *Gold Bull.* **2004**, *37*, 72–133.
[11] A. Abad, P. Concepcion, A. Corma, H. Garcia, *Angew. Chem.* **2005**, *117*, 4134–4137; *Angew. Chem. Int. Ed.* **2005**, *44*, 4066–4069.
[12] A. C. Gluhoi, N. Bogdanchikova, B. E. Nieuwenhuys, *J. Catal.* **2005**, *229*, 154–162.
[13] M. D. Hughes et al., *Nature* **2005**, *437*, 1132–1135.
[14] T. A. Nijhuis, M. Makkee, J. A. Moulijn, B. M. Weckhuysen, *Ind. Eng. Chem. Res.* **2006**, *45*, 3447–3459.
[15] a) T. V. W. Janssens, B. S. Clausen, B. Hvolbæk, H. Falsig, C. H. Christensen, T. Bligaard, J. K. Nørskov, *Top. Catal.* **2007**, *44*, 15–26; b) N. Lopez, T. V. W. Janssens, B. S. Clausen, Y. Xu, M. Mavrikakis, T. Bligaard, J. K. Nørskov, *J. Catal.* **2004**, *223*, 232–235.
[16] C. H. Christensen, B. Jørgensen, J. Rass-Hansen, K. Egeblad, R. Madsen, S. K. Klitgaard, S. M. Hansen. M. R. Hansen, H. C.

Andersen, A. Riisager, *Angew. Chem.* **2006**, *118*, 4764 – 4767; *Angew. Chem. Int. Ed.* **2006**, *45*, 4648 – 4651.
[17] R. Burch, *Phys. Chem. Chem. Phys.* **2006**, *8*, 5483 – 5500.
[18] M. J. Lippits, A. C. Gluhoi, B. E. Nieuwenhuys, *Top. Catal.* **2007**, *44*, 159 – 165.
[19] L. Gang, B. G. Anderson, J. van Grondelle, R. A. van Santen, *Appl. Catal. B* **2003**, *40*, 101 – 110.
[20] M. Haruta, *Catal. Today* **1997**, *36*, 153 – 166.
[21] B. Hammer, *Top. Catal.* **2006**, *37*, 3 – 16.
[22] C. Xu, J. Su, X. Xu, P. Liu, H. Zhao, F. Tian, Y. Ding, *J. Am. Chem. Soc.* **2007**, *129*, 42 – 43.
[23] B. Jürgens, C. Kübel, C. Schultz, T. Nowitzki, V. Zielasek, J. Biener, M. M. Biener, A. V. Hamza, M. Bäumer, *Gold Bull.* **2007**, *40*, 142 – 148.
[24] P. Atkins, J. de Paula, *J. Physical Chemistry* , 8th ed. Oxford University Press, Oxford, **2006**.
[25] J. K. Nørskov et al., *J. Catal.* **2002**, *209*, 275 – 278.
[26] T. Bligaard, J. K. Nørskov, S. Dahl, J. Matthiesen, C. H. Christensen, J. Sehested, *J. Catal.* **2004**, *224*, 206 – 217.
[27] J. Wintterlin, S. Völkening, T. V. W. Janssens, T. Zambelli, G. Ertl, *Science* **1997**, *278*, 1931 – 1933.
[28] Z.-P. Liu, P. Hu, *Top. Catal.* **2004**, *28*, 71 – 78.
[29] A. Eichler, J. Hafner, *Surf. Sci.* **1999**, *433*, 58 – 62.
[30] B. E. Nieuwenhuys, *Surf. Rev. Lett.* **1996**, *3*, 1869 – 1888.
[31] L. Grabow, Y. Xu, M. Mavrikakis, *Phys. Chem. Chem. Phys.* **2006**, *8*, 3369 – 3374.
[32] A. Carlsson, A. Puig-Molina, T. V. W Janssens, *J. Phys. Chem. B* **2006**, *110*, 5286 – 5293.
[33] G. Mills, M. S. Gordon, H. Metiu, *J. Chem. Phys.* **2003**, *118*, 4198 – 4205.
[34] Z.-P. Liu, P. Hu, A. Alavi, *J. Am. Chem. Soc.* **2002**, *124*, 14770 – 14779.
[35] L. M. Molina, B. Hammer, *Phys. Rev. B* **2004**, *69*, 155424.

